RESEARCH ARTICLE
Cytoskeleton, February 2014 71:119–135 (doi: 10.1002/cm.21156)

Adhesion-Dependent Modulation of Actin Dynamics in Jurkat T Cells

King Lam Hui,[1] Sae In Kwak,[2] and Arpita Upadhyaya[1,3]*

[1]Department of Physics, University of Maryland, College Park, Maryland 20742
[2]Department of Chemistry and Biochemistry, University of Maryland, College Park, Maryland 20742
[3]Institute for Physical Science and Technology, University of Maryland, College Park, Maryland 20742

Received 9 June 2013; Revised 21 October 2013; Accepted 29 October 2013
Monitoring Editor: Pekka Lappalainen

Contact formation of T cells with antigen presenting cells results in the engagement of T cell receptors (TCRs), recruitment and aggregation of signaling proteins into microclusters and ultimately, T cell activation. During this process, T cells undergo dramatic changes in cell shape and reorganization of the cytoskeleton. While the importance of the cytoskeleton in T cell activation is well known, the dynamics of the actin cytoskeleton and how it correlates with signaling clusters during the early stages of spreading is not well understood. Here, we used total internal reflection fluorescence microscopy to study the dynamics of actin reorganization during Jurkat T cell spreading and the role of integrin ligation by the adhesion molecule, vascular cell adhesion molecule (VCAM), in modulating actin dynamics. We found that when T cells spread on anti-CD3 antibody-coated glass surfaces, the cell edge exhibited repeated protrusions and retractions, which were driven by wave like patterns of actin that emerged from signaling microclusters. Addition of VCAM on the activating substrate altered the dynamics of actin both globally and locally, leading to a smooth expansion of the cell edge and the disappearance of waves. Our results suggest that the actin cytoskeleton in Jurkat cells is capable of organizing into spatial patterns initiated by TCR signaling and regulated by integrin signaling. © 2013 Wiley Periodicals, Inc.

Key Words: lymphocytes; actin waves; integrins; total internal reflection fluorescence

Introduction

Cellular responses to environmental stimuli involve large-scale changes in morphology, primarily driven by reorganization of the actin cytoskeleton [Janmey and McCulloch, 2007; Kasza et al., 2007; Kasza and Zallen, 2011]. One striking example of this occurs during cell-cell recognition in immune cells, where T lymphocytes rapidly spread to establish contacts with antigen-presenting cells (APCs) [Monks et al., 1998; Wulfing and Davis, 1998; Grakoui et al., 1999]. These contacts allow T cell receptors (TCRs) to bind antigen molecules displayed on the APC surface. Antigen binding results in the activation of TCRs and the formation of signaling microclusters that consist of activated TCR and various downstream signaling molecules [Bunnell et al., 2002; Campi et al., 2005; Douglass and Vale, 2005; Yokosuka et al., 2005; Varma et al., 2006]. TCR activation also initiates signaling pathways, which activate actin nucleation-promoting factors (NPFs) such as WAVE2, HS1, and WASP [Billadeau et al., 2007]. These NPFs in turn activate the Arp2/3 complex, nucleating actin polymerization, which provides the necessary force for membrane deformation, cell spreading, and microcluster transport [Billadeau et al., 2007; Burkhardt et al., 2008; Beemiller and Krummel, 2010; Dustin and Groves, 2012]. Previous work demonstrating the importance of the actin cytoskeleton for T cell activation has focused on the later stages of spreading when fully spread cells have established a lamellipodial actin network [Bunnell et al., 2001; Yokosuka et al., 2005; Gomez et al., 2006; Nolz et al., 2006; Kaizuka et al., 2007; Yu et al., 2010; Babich et al., 2012; Beemiller et al., 2012; Smoligovets et al., 2012; Yi et al., 2012]. However, extensive signaling, accompanied by the recruitment of NPFs at nascent microclusters [Barda-Saad et al., 2005] is initiated within a minute of contact [Houtman et al., 2005]. The relationship between Arp2/3-mediated actin dynamics and the spatiotemporal organization of TCR microclusters during this early phase of spreading is not well understood.

Arp2/3-nucleated actin polymerization has been intensely studied in many cell types owing to its importance in chemotaxis, cell motility, endocytosis, membrane ruffling, and ventral F-actin waves [Welch and Mullins, 2002; Goley and Welch, 2006; Soderling, 2009]. These studies show that

Additional Supporting Information may be found in the online version of this article.

*Address correspondence to: Arpita Upadhyaya; Institute for Physical Science and Technology, Bldg. 85, University of Maryland, College Park MD 20742. E-mail: arpitau@umd.edu

Published online 31 December 2013 in Wiley Online Library (wileyonlinelibrary.com).

polymerizing actin can form stationary or moving spots, or propagate as waves under a broad variety of conditions. In particular, ventral F-actin waves have been extensively observed in neutrophils [Weiner et al., 2007], *Dictyostelium* [Vicker, 2002; Bretschneider et al. 2004, 2009; Gerisch et al., 2009; Schroth-Diez et al., 2009] and adherent cells [Case and Waterman, 2011] suggesting that the underlying mechanisms of their formation are largely conserved. In adherent cells, these actin structures facilitate integrin binding to the extracellular matrix and the assembly of integrin-associated protein clusters, highlighting their potential to organize membrane receptors and associated signaling proteins at cell-substrate contacts. However, despite the engagement of a similar complement of actin regulators as other cells, it is not known if T cells exhibit such dynamic structures and whether these play a role in microcluster assembly.

Here, we have used multimodal live cell imaging to quantitatively study the dynamics of actin in relation to signaling microclusters during early spreading in Jurkat T cells. We find that actin organizes into spatiotemporal patterns such as traveling waves and spirals, which are driven by polymerization. We find several distinct features of actin structures in T cells. First, TCR activation is required for their generation. Consequently, we find that the waves arise from discrete foci, marked by microclusters. Second, the actin waves in T cells appear to be associated with moving membrane folds suggesting that a coupling between chemical and mechanical factors is required to generate these waves. Finally, these waves appear to be regulated by the level of adhesion, as integrin-mediated adhesion to stimulatory substrates suppressed wave formation, restricting nascent actin polymerization to the cell periphery. In addition to global changes in actin dynamics, integrin-mediated adhesion also altered the assembly and disassembly kinetics of actin in the vicinity of signaling clusters. The alterations in actin dynamics correlated with changes in amplitudes of signaling clusters. Our studies demonstrate an intricate relationship between F-actin dynamics, local signaling, and integrin-mediated adhesion during activation and spreading of Jurkat T cells and may have implications for theoretical models of actin dynamics.

Results

Cell Membrane Dynamics during Jurkat T Cell Spreading

Jurkat T cells expressing EGFP-actin were allowed to contact a glass substrate coated with anti-CD3 antibody and imaged with interference reflection microscopy (IRM) and total internal reflection fluorescence (TIRF) microscopy. Within seconds of incubation, cells formed contacts with the coated substrate, which could be identified as fluctuating light and dark IRM patterns and interference rings. Following initial contact, the cells spread, rapidly increasing their contact area (Fig. 1A). Simultaneously collected time-lapse TIRF images of EGFP-actin (Fig. 1B) showed that the leading edge was associated with radially moving fronts of actin. Figure 1D shows a traveling bump of actin intensity at the cell periphery as it moved radially outwards. Kymographs (Fig. 1C) show that the cell edge underwent repeated protrusions and retractions throughout spreading before establishing a clear lamellipodium, which was marked by the formation of a ring of actin and the establishment of retrograde flow. The protrusion-retraction events were not strictly periodic, and the average time interval between successive protrusion peaks was 80 ± 17s ($N = 56$ intervals from 10 cells). Successive cell contours extracted from the IRM images (Fig. 1E) also show that the cell edge around the entire cell periphery was dynamic with extensive protrusions and retractions. The time evolution of the leading-edge position as obtained from the IRM images was tracked using a level-set method [Machacek and Danuser, 2006] to determine the local protrusion and retraction velocities normal to the leading edge. A relatively irregular sequence of protrusion and retraction events was observed with typical velocities on the order of 100–120 nm/s (Fig. 1F).

While similar oscillations have been observed in primary T cells spreading on stimulatory bilayer substrates [Dobereiner et al., 2006], the relationship between actin and edge dynamics is not well understood. To quantify this, we calculated the intensity profile of EGFP-actin by summing the intensity of pixels within a 2 μm band around the cell edge obtained from the IRM images (Fig. 1G). Brighter F-actin intensities appeared to weakly correlate with slower protrusion velocities while lower intensities were associated with larger protrusion velocities. To further quantify the relationship, we computed auto- and cross-correlations of the edge velocity and the local actin signal. While the temporal autocorrelation of the leading edge velocity and actin intensity showed a pronounced dip, the cross-correlation indicated a slight offset of ~15 s (Fig. 1H). This indicates that the leading edge velocity peaks several seconds (15 ± 4s, $n = 5$ cells) earlier than the actin intensity, similar to observations in adherent cells [Ryan et al., 2012a].

Actin Waves during Early Spreading of Jurkat T Cells

In addition to the peripheral actin waves (Fig. 2A), we also observed dynamic actin structures interior to the cell periphery, such as traveling waves moving radially outwards and inwards towards the cell center (Figs. 2B and 2C), as well as spiral patterns (Fig. 2C; Supporting Information, Movie S1). The movement of these structures was visualized as shown in a representative kymograph (Fig. 2D). The average velocity for the entire population was 7.1 ± 2.0 μm/min ($n = 80$, Fig. 2E) consistent with the

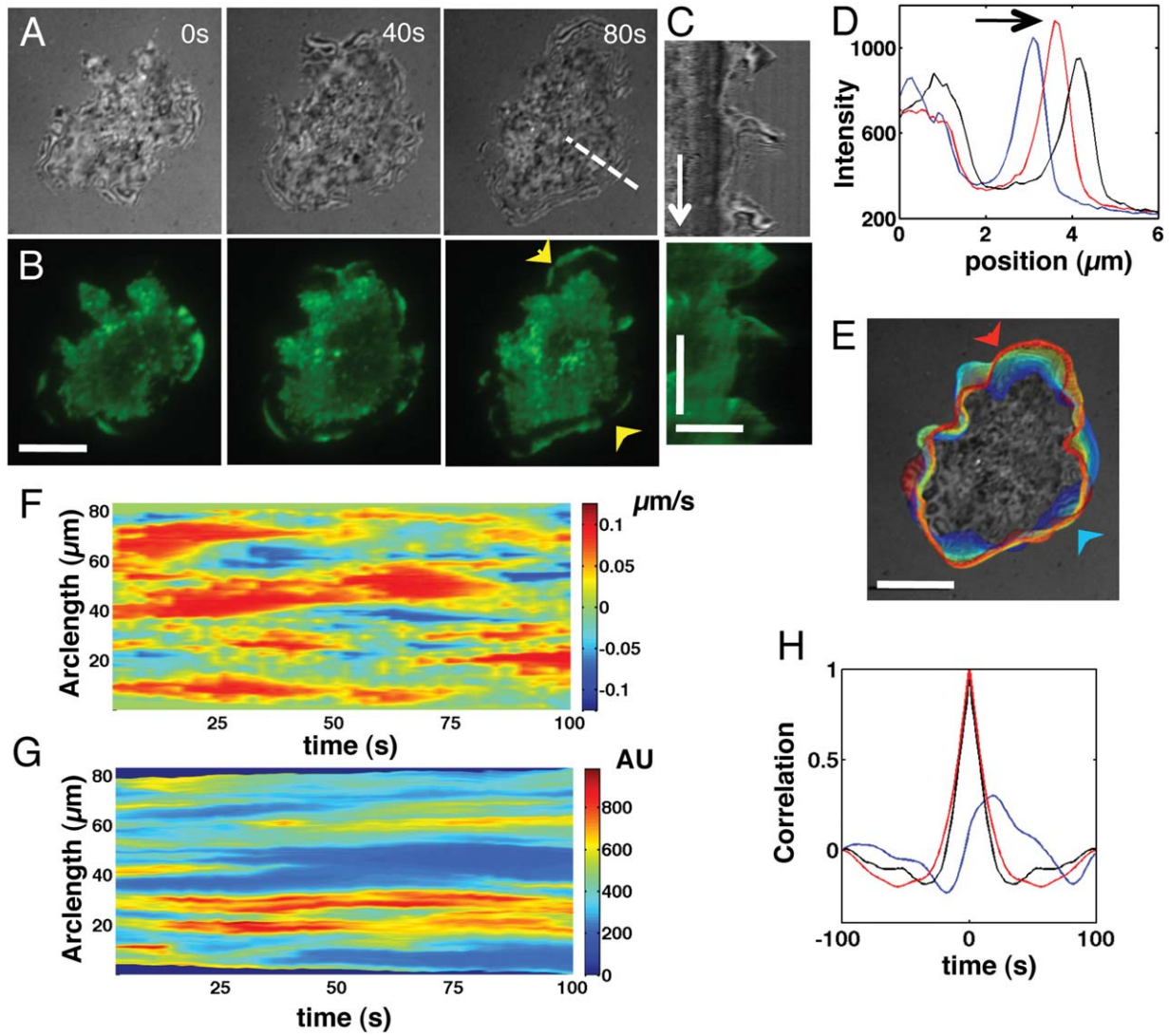

Fig. 1. Spreading T cells display dynamic edge movement and actin waves. (**A**) Time-lapse IRM images of a Jurkat T cell spreading on anti-CD3-coated substrates. (**B**) Time-lapse TIRFM images of the same cell showing peripheral actin waves, which protrude and retract (as marked by the yellow arrows). Scale bar is 10 μm. (**C**) Kymograph of a radial line across the cell edge (dashed line in (A)) in IRM (top) and TIRF (bottom) showing repeated protrusions and retractions. Scale bars: horizontal 5 μm; vertical 2 min. (**D**) Line profile of actin intensities at three different times (12 s apart) showing a traveling "bump" of actin moving radially outward at the cell edge. Line profile corresponds to the wave marked by the top yellow arrow in (B). Direction of the arrow corresponds to time. (**E**) Cell outlines at multiple time-points in different colors, going from blue (earlier in time) to red (later in time) for 0 to 5 min. The arrows mark representative spots of protrusion and retraction. (**F**) Heat map showing the edge velocity computed from IRM images in the normal direction along the cell edge. Warm colors indicate protrusions and cool colors indicate retractions. (**G**) Heat map of actin intensities along the cell perimeter as a function of time. Warm colors represent higher actin intensities. (**H**) Average correlation coefficients for the temporal autocorrelation of leading edge velocity (black), temporal autocorrelation of EGFP-actin intensity (red), and temporal cross-correlation of leading edge velocity with EGFP-actin intensity (blue).

edge velocities observed in Fig. 1F. Internal actin structures typically had an average velocity of 6.7 ± 2.1 μm/min ($n = 27$), similar to that of the peripheral actin waves, 7.1 ± 1.8 μm/min ($n = 43$), suggesting that all these structures may be driven largely by actin polymerization and share a similar mechanistic origin.

Previous studies have reported the assembly of actin or actin nucleators into wave-like structures of protein density in a variety of cell types, such as neutrophils, *Dictyostelium*, and epithelial cells [Bretschneider et al., 2004, 2009; Gerisch et al., 2004, 2009; Weiner et al., 2007; Asano et al., 2008; Case and Waterman, 2011]. To examine whether the internal waves we observed were actin density waves, we stably transfected EGFP-actin labeled Jurkat cells with TagRFP-T as a cytosolic marker to generate two-color cell lines. TIRF images of the red fluorescence show the position of the membrane, which is in closest contact with the substrate, as the TIRF signal disappears when the membrane-substrate distance increases. Dual-wavelength TIRF imaging of actin and cytosol showed a high degree

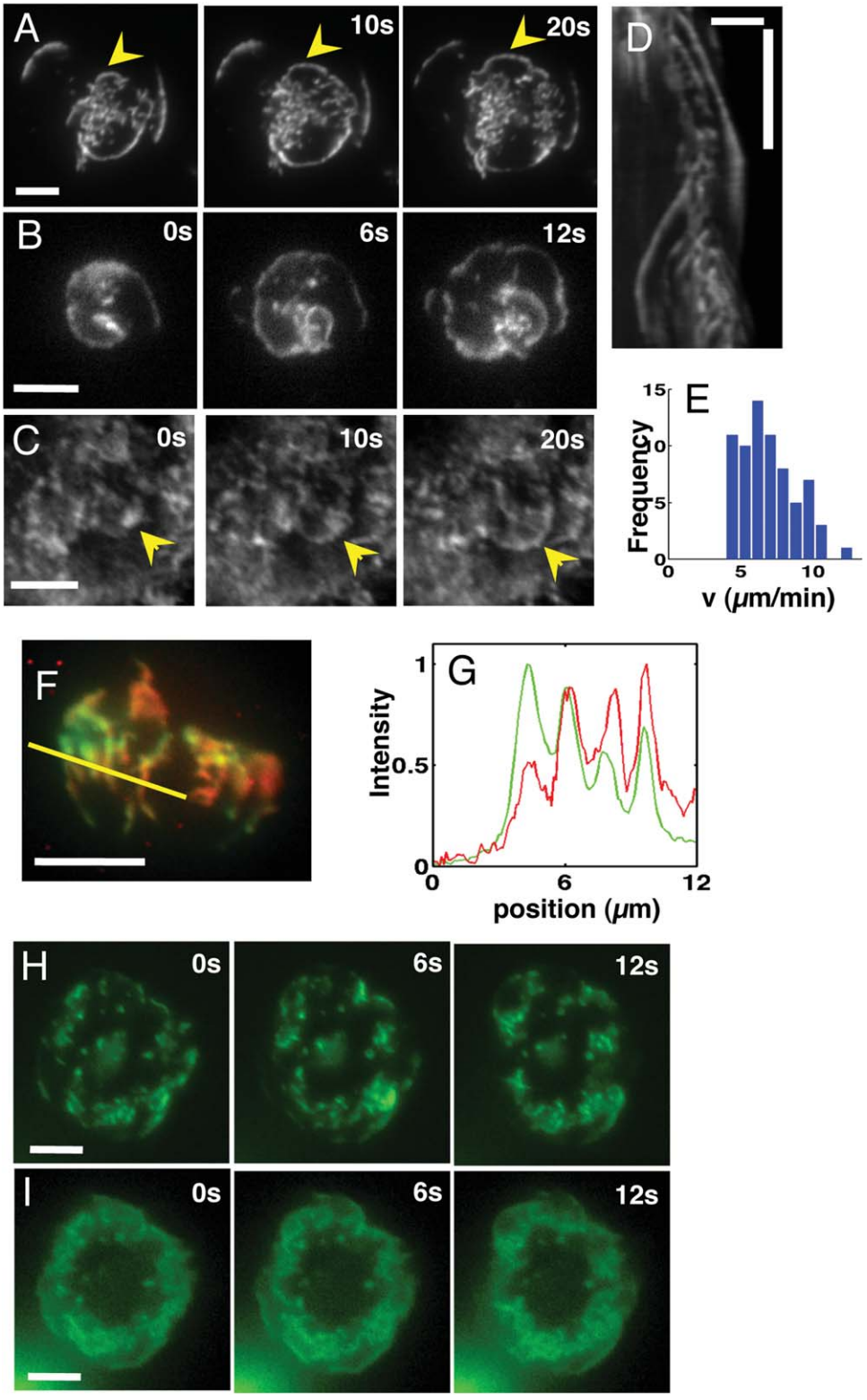

Fig. 2.

of correlation between the location of actin waves (green) and cytosol (red), which likely corresponds to membrane folds (Fig. 2F; Supporting Information, Movie S2). Direct observation of the membrane by labeling proved to be difficult owing to membrane recycling over the time-scale of spreading. Line profiles of the fluorescence intensities across a region of the cell plotted for the two channels show that the peaks of intensities overlap with each other, indicating that actin is colocalized with membrane folds that are in close contact with the surface (Fig. 2G). We next examined

whether for some of the folds the actin peaks corresponded to density waves. We drew evenly spaced radial intensity profiles (6 per cell, 10 cells) around the cell perimeter and normalized the radial intensity profiles for both the actin and Tag-RFP channels to their respective local maxima along the profile and computed the ratio of the relative actin intensity to that of the cytosol. A ratio greater than 1 would indicate an actin density wave. We found that across multiple cells, each radial profile was associated with at least one peak where the ratio was greater than 1, that is, the relative actin intensity was higher than the relative cytosolic intensity. Across the population, we observed that 50% of the actin peaks had a relative ratio greater than 1 indicating that these were actin density peaks. In addition to TIRF, we observed actin/membrane structures in simultaneously collected epifluorescence images (Fig. 2H and Supporting Information, Movie S3), suggesting that these waves were not a proximity artifact of TIRF imaging. Taken together, these observations suggest that the observed waves are a mixture of coupled actin-membrane waves as well as actin density waves traveling on a planar membrane surface. This is consistent with our previous observations using IRM that the membrane topography at the cell substrate interface is not entirely flat, rather it has vertical undulations on the order of 25–50 nm that are about a micron in length [Lam Hui et al., 2012].

We next verified that these actin waves result from TCR activation at the surface to formally rule out the possibility that these structures accompany passive spreading. We imaged cells spreading on substrates coated with the proadhesive ligand, anti-CD43, which leads to non-integrin mediated adhesion, without any stimulatory anti-CD3. While cells spread on this surface (though to a smaller extent than on stimulatory antibody), the actin cytoskeleton as imaged in TIRF remained largely uniform with no visible structures such as the propagating waves observed on an activating surface (Supporting Information, Figs. S1A and S1B). The advance of the cell periphery was slower and not as smooth and efficient as in the presence of stimulatory antibody. These results suggest that the actin structures are dynamically stabilized membrane folds that require TCR activation and signaling for their formation and maintenance.

Actin Dynamics at Signaling Microclusters

TCR activation leads to the formation of signaling microclusters and activation of actin polymerization [Barda-Saad et al., 2005; Nolz et al., 2006; Zipfel et al., 2006]. To examine the spatial relation between signaling clusters and actin dynamics, we established Jurkat T cell lines stably expressing both EYFP-ZAP70 (a tyrosine kinase that directly binds to phosphorylated zeta-chains on activated TCRs) and TagRFP-T-actin and used dual-wavelength TIRF microscopy to visualize actin and microcluster dynamics during the early phase of spreading. We found that ZAP70 clusters appeared at the very first points of contact that the cell makes with the substrate (Fig. 3A). The initial appearance of ZAP70 was associated with an actin cloud, which moved radially outwards as a wave front (Supporting Information, Movie S4). As the cell spread, new clusters were formed at the actin-rich periphery (Supporting Information, Movie S4). We next examined whether actin waves emerged in the vicinity of newly formed clusters. Figure 3B shows a single cluster (yellow arrowhead) from the vicinity of which multiple actin waves emerge. The intensity profiles corresponding to the dashed line at 0 s show the formation of a cluster (arrowhead) and emergence of actin waves (arrow) near the cluster (Fig. 3C). This example is representative of at least 30 such instances for 20 cells across four independent experiments. A three-color image showing a wave of actin at three successive time intervals (R, G, and B successively) separated by 3 s each clearly shows emerging waves (Fig 3D). Figure 3E shows the intensity profiles along the dashed yellow line in Fig. 3D with R, G, and B representing three successive times. The dashed lines correspond to ZAP70 fluorescence indicating a cluster, and the solid lines represent actin intensity. As in Fig. 3C, we note that a wave of actin (a bump in the intensity peak) appears close to the cluster and propagates outward (arrowhead), while a second wave of actin emerges (arrow). Figure 3F shows a third similar example. Our observations are consistent with FRET experiments showing the accumulation of Arp2/3 regulators and Rho-GTPases that lead to actin nucleation [Barda-Saad et al., 2005].

Fig. 2. Spreading Jurkat T cells display membrane coupled actin waves. (**A**) Time-lapse image of EGFP-actin expressing cell on anti-CD3-coated substrates showing peripheral actin waves. (**B**) Time-lapse image showing a spiral wave of actin. (**C**) Time-lapse TIRF images showing internal actin waves. (**D**) Kymograph showing multiple types of propagating actin structures. The linear streaks of GFP represent traveling waves. (**E**) Histogram of actin wave velocities across cell populations. The mean velocity is 7.1 ± 2.0 μm/min, $N = 80$. (**F**) Dual-wavelength images showing snapshots of a spreading cell with EGFP-labeled actin (green) and TagRFP-T-labeled cytosol (red). A high degree of correlation between the patterns in the red and green channels show that actin is colocalized with membrane structures, indicating that waves correspond to membrane folds. (**G**) Intensity profiles along the line shown in (F) in the red and green channels show a close correspondence between the peaks in the two colors further demonstrating colocalization between actin and membrane. Horizontal scale bars are 5 μm and vertical scale bar in (D) is 1 min. (**H**) Time-lapse TIRF images of EGFP-actin cell showing propagating actin waves. (**I**) Corresponding epifluorescence images of the same cell showing that waves are visible in wide field fluorescence as well. Scale bar is 5 μm.

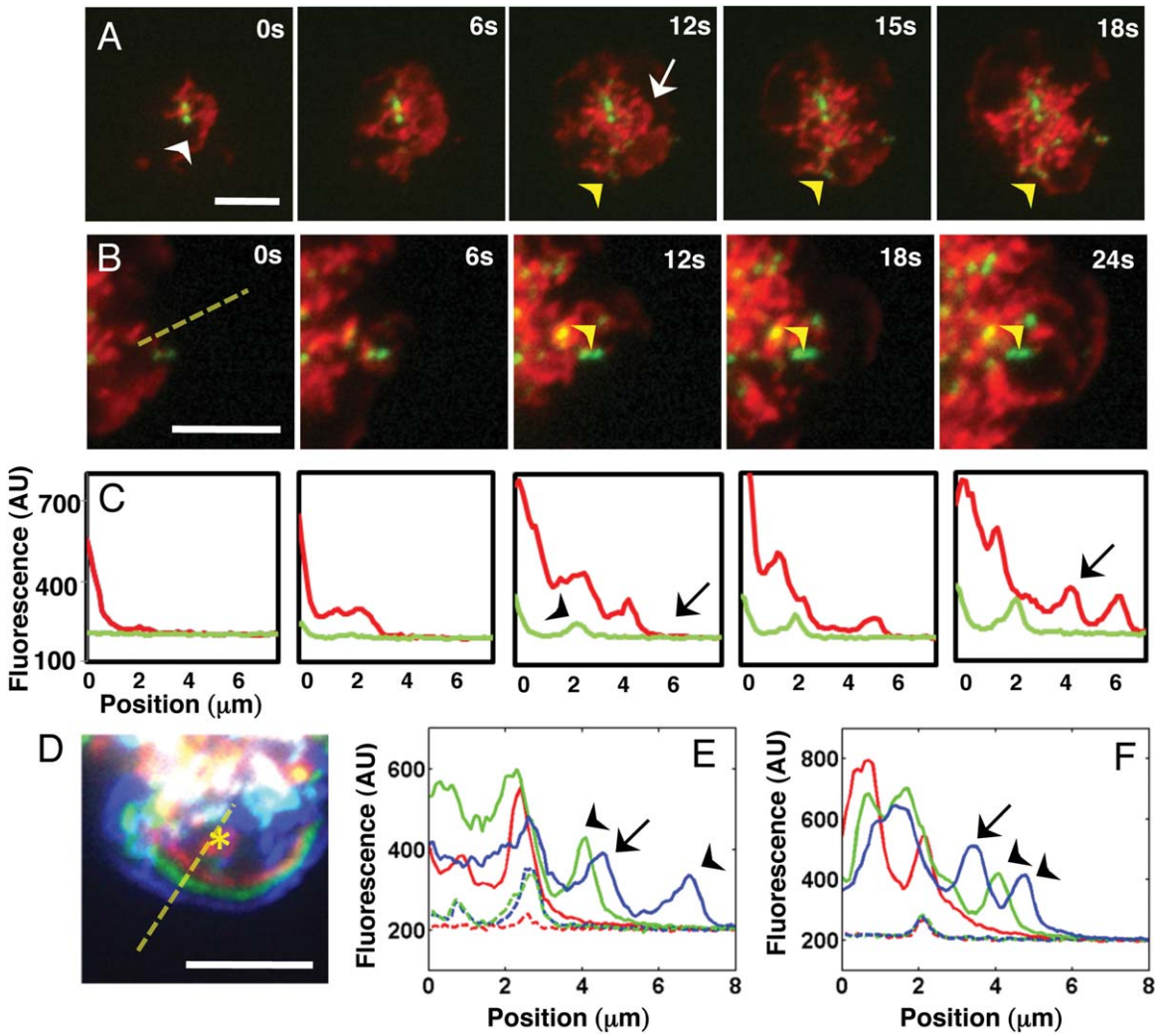

Fig. 3. Actin waves at signaling microclusters. (**A**) Time-lapse TIRF images of cells dual-labeled with EYFP-ZAP70 (green) and TagRFP-T-actin (red) spreading on an anti-CD3-coated substrate at the indicated times. The first three images show waves emerging from the earliest clusters. The white arrow at 12 s shows the emergence of a second and third successive actin wave from the same initial clusters. Yellow arrowheads show the formation of clusters at the edges of a propagating actin wave. Scale bar: 5 μm. (**B**) A zoomed in section of a dual labeled cell showing multiple actin waves emerging from a ZAP70 cluster (yellow arrowhead). Scale bar: 5 μm. (**C**) Line profile along the dashed line in panel 1 of (C) with EYFP intensity in green and TagRFP-T intensity in red. Images are 6 s apart. Arrowhead in panel 3 marks the appearance of a nascent ZAP70 cluster that grows in intensity. An actin wave emerges from the cluster as seen by the appearance of a new peak in actin intensity in the last panel in (C). (**D**) A pseudocolor image showing a wave of actin at three times (R, G, and B successively) separated by 3 s each. The asterisk represents the position of a ZAP70 cluster. Scale bar is 5 μm. (**E**) Intensity profiles of EYFP-ZAP70 fluorescence (dashed lines) and TagRFP-T-actin fluorescence (solid lines) along the dashed yellow line in D with R, G, and B representing three successive times 9 s apart. Arrowhead marks the first actin wave and arrow marks the second actin wave emerging near the cluster. (**F**) Intensity profiles along of EYFP-ZAP70 and TagRFP-T-actin fluorescence along another radial section of a cell showing the emergence of actin waves near a cluster.

Distribution of Actin Regulators during Early Spreading

Studies in neutrophils and *Dictyostelium* have shown that ventral F-actin waves contain Arp2/3 and its activator, the WAVE complex, suggesting their involvement in stimulating actin treadmilling [Bretschneider et al., 2004; Weiner et al., 2007]. To determine whether members of the WAVE complex, which link Rac signaling downstream from activated TCRs to actin nucleation [Zipfel et al., 2006] play a role in generation of the actin structures in T cells, we focused on Abi1. Abi1 is believed to activate actin polymerization through its regulation of N-WASP and WAVE [Innocenti et al., 2005]. Previous studies have shown that Abi1 accumulates at the leading edge of spreading Jurkat cells [Zipfel et al., 2006] but whether it is involved in the generation and maintenance of actin waves is not known. We transiently transfected E6-1 Jurkat cells, wildtype or stably expressing TagRFP-T-actin, with EYFP-Abi1 and imaged them on anti-CD3-coated coverslips during spreading.

EYFP-Abi1 rapidly accumulated at the leading edge of spreading cells and localized to a thin region at the tips of the advancing lamellipod, followed by actin dense regions (Fig. 4A, Supporting Information, Movie S5). Abi1 was localized more proximal to the cell leading edge, as shown by the line profile of Abi1 (green) and actin (red) taken from a representative snapshot of a spreading cell (Figs. 4B and 4C). Often multiple fronts of traveling waves were observed to originate from the same location and propagate outwards (Figs. 4D and 4E). The intensity profile shows the progression of the first wavefront in time and the appearance of a second one. In addition to being localized at the leading front of waves, Abi1 was observed in discrete locations distributed throughout the cell contact zone in clusters from which the waves emerged (Fig. 4F, Supporting Information, Movie S6). These results indicate that the structures that we observe are likely membrane folds that are dynamically stabilized by Arp-2/3-mediated actin polymerization activated by the WAVE complex.

Perturbations of the Acto-Myosin Cytoskeleton

To more directly implicate the active contribution of actin polymerization to the propagation of these waves, we treated cells (labeled with EYFP-Abi1 and TagRFP-T-actin) with the drug Latrunculin-A (Lat-A), which sequesters actin monomers and hence inhibits actin polymerization. Addition of 250 nM or more Lat-A to cells 1–2 min after the initiation of spreading arrested the leading edge advance and caused a loss of repeated protrusion/retraction activities (Figs. 5A and 5B). This was accompanied by an overall reduction in the levels of Abi1 and actin fluorescence as the actin and Abi1 waves were disrupted (Figs. 5C and 5D). Low doses of Lat-A (100 nM) reduced the wave speeds from 8.8 ± 1.9 μm/min (control) to 2.7 ± 0.7 μm/min (Fig. 5E), suggesting that actin polymerization drives the wave movement. When cells were treated with 1 μM Jasplakinolide (Jasp), which stabilizes actin filaments and inhibits both polymerization and depolymerization [Bubb et al., 1994], the peripheral and internal waves were abolished (Fig. 5F). The repeated protrusion and retraction dynamics of the cell edge was also inhibited in the presence of Jasp. The cell periphery continued to expand outwards but at a slower rate than in the absence of the drug (Fig. 5G). These observations suggest that actin waves are driven by polymerization and depolymerization of actin originating from localized regions enriched in actin regulatory proteins.

We next examined the role of myosin contractility in the generation or propagation of these waves. The primary form of myosin II present in T cells is myosin IIA with a very small fraction of myosin IIB [Jacobelli et al., 2004; Ilani et al., 2009]. We used siRNA to suppress the expression of myosin IIA heavy chain (Myh9) in EGFP-actin expressing Jurkat cells. We found that these cells depleted in Myosin IIA activity spread similar to wild-type cells. The formation, propagation, and duration of actin waves in these cells were qualitatively similar to wild type cells (Fig. 5H, Supporting Information, Movie S7), and the speed of actin waves was measured to be 8.2 ± 3.5 μm/min, not significantly different from control EGFP-actin cells ($P > 0.1$, Wilcoxon rank-sum test). Consistent with this, we found that addition of 50 μM blebbistatin (an inhibitor of non-muscle myosin IIA activity) to TagRFP-T-actin expressing cells also did not inhibit actin waves.

Vascular Cell Adhesion Molecule Modulates the Dynamics of the Cell Membrane and Actin Waves

While TCR activation generates rapid signaling, these events are transient. Sustained activation of T cells requires additional costimulatory signals such as through integrins. In particular, the integrin, VLA-4 ($\alpha_4\beta_1$), facilitates T cell adhesion and binding with its ligand vascular cell adhesion molecule (VCAM)−1 leads to costimulation of T cell activation [Udagawa et al., 1996; Doucey et al., 2003; Nguyen et al., 2008]. VLA-4 ligation may regulate actin dynamics through its effect on the adaptor protein, SLP-76 and the Rac-GTPase, Vav [Wu et al., 1996; Nguyen et al., 2008]. To examine the role of VCAM in actin reorganization and signaling dynamics during early spreading, we coated glass coverslips with 5 μg/mL VCAM in addition to 10 μg/mL anti-CD3 antibody. Cells dropped onto these substrates formed contacts as seen in IRM and spread out over the surface (Fig. 6A). In contrast to control cells, the cell periphery advanced smoothly outwards without undergoing protrusions and retractions. Furthermore, the cell substrate interface was much flatter on VCAM-coated substrates as seen by the uniform gray intensity of the IRM images differing from the control cells that exhibit large variations in IRM intensity at the contact zone. Finally, TIRF imaging showed a smooth accumulation of actin at lamellipodia, which formed a ring at the periphery as the cell edge advanced (Fig. 6B; Supporting Information, Movie S8). We noted that the rich dynamics of peripheral and internal actin waves as described for the control case were not observed in the presence of VCAM. Kymograph analysis of both the IRM and TIRF images further emphasized the smoothness of the edge progression (Figs. 6C and 6D). Data shown are representative of at least 20 cells across five independent experiments.

A plot of successive cell contours showed that the cell periphery moved out in a uniform manner (Fig. 6E) without protrusions and retractions. Accordingly, the heat map plot of velocities shows a uniform outward protrusion of the cell edge (Fig. 6F) but with a larger overall edge velocity compared to control cells. The temporal autocorrelation (Fig. 6G red curve) of the edge velocity showed a long correlation time, consistent with the smooth expansion of the cell edge while the actin intensity (Fig. 6G black curve) became uncorrelated within 20 s. The relationship between

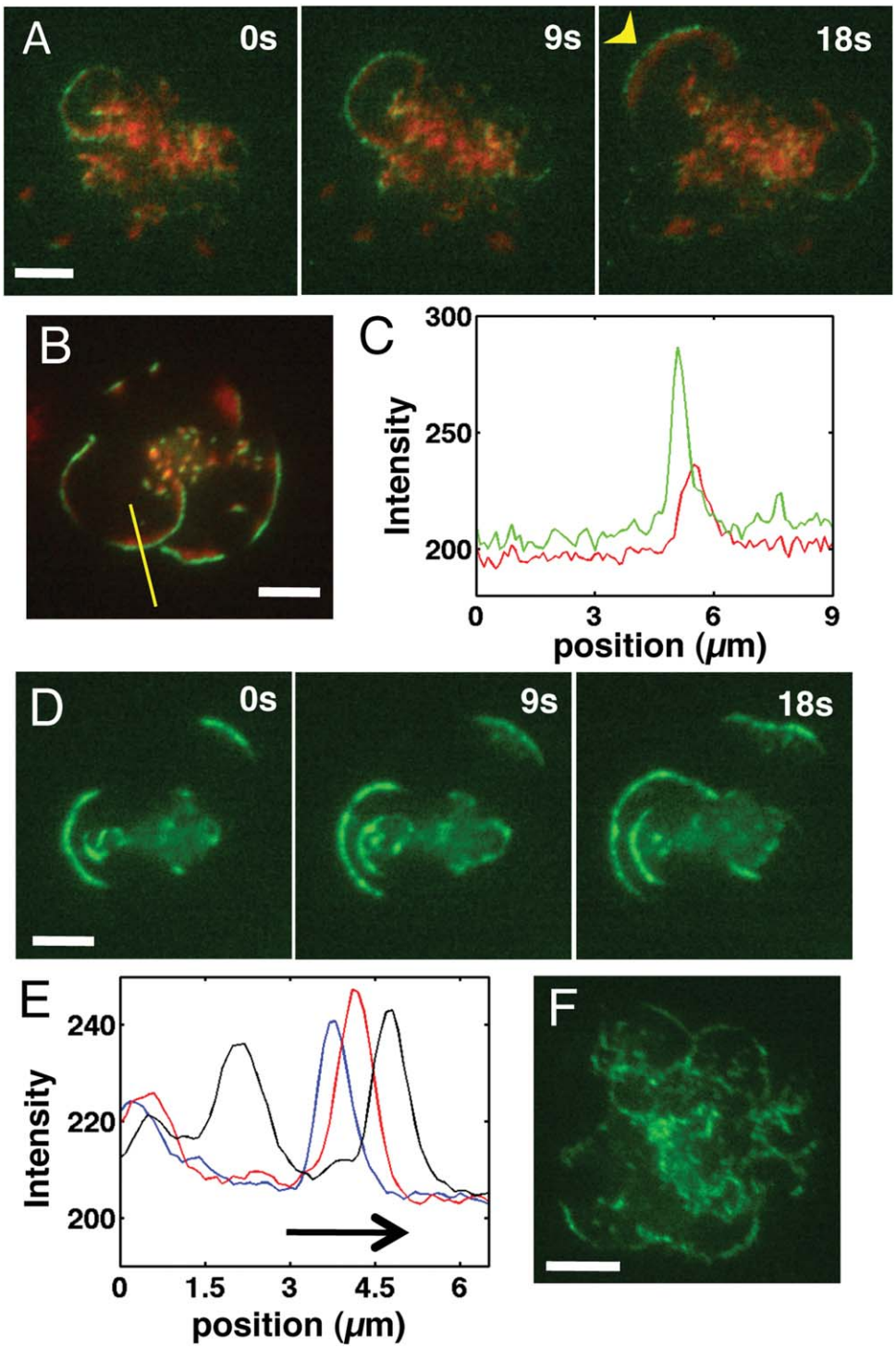

Fig. 4. Abi1 nucleates actin polymerization at the leading edge of waves. (**A**) Time-lapse images of a dual-color cell expressing EYFP-Abi1 and Tag-RFP-T-actin spreading on anti-CD3 coated glass. Images show the accumulation of EYFP-Abi1 at the very edge of the membrane followed by actin at the lamellipodia. (**B**) A two-color snapshot of a dual-labeled cell in the process of spreading. (**C**) Fluorescence intensity profile along the yellow line across the cell edge in (B) shows Abi (green) as a sharp front and a broader actin (red) intensity profile, which follows the Abi1 peak. 0 on the *x*-axis of the graph corresponds to the outer end of the line drawn in (B). (**D**) Time-lapse images of a spreading EYFP-Abi1-labeled cell showing the emergence of multiple successive waves from a single focal point. (**E**) Three intensity profiles at successive time intervals, showing the movement of a traveling "bump" of Abi1 fluorescence. Note a second peak appears indicating the formation of a second traveling wave. The direction of the arrow represents the progression of time. (**F**) A snapshot of a spread cell showing the distribution of EYFP-Abi1 in localized regions throughout the cell substrate contact zone.

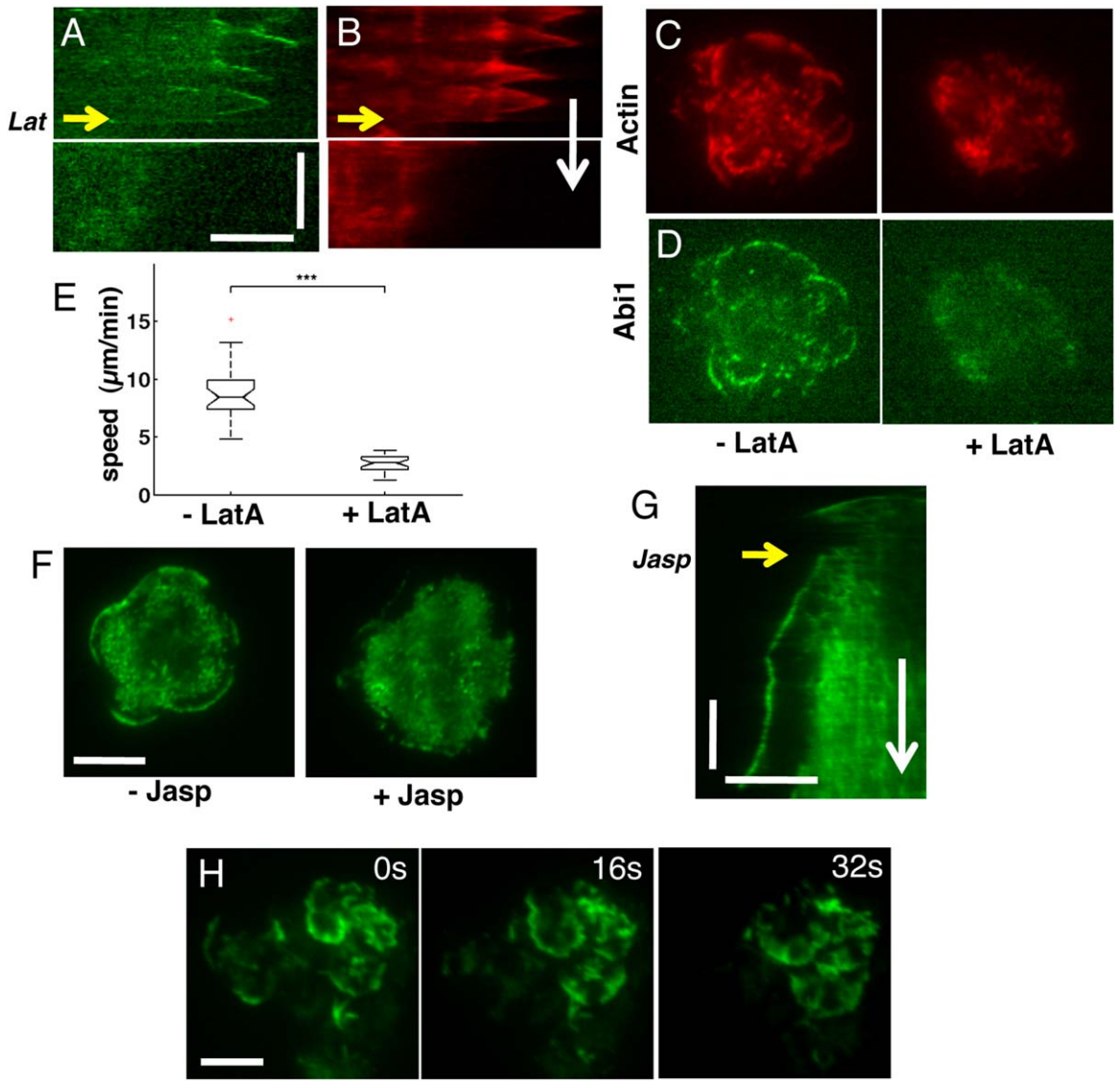

Fig. 5. The role of the actomyosin cytoskeleton in actin waves. (**A**, **B**) Kymographs along a radial line of a cell labeled with EYFP-Abi1 (green) and TagRFP-T-actin (red), shows that the addition of Lat-A (250 nM), at the time indicated by the yellow arrow, inhibits the protrusions and retractions of the cell edge. Horizontal scale bar: 5 μm. Vertical scale bar: 2 min. (**C**, **D**). Snapshots of a cell labeled with EYFP-Abi1 (green) and TagRFP-T-actin (red), showing the presence of actin waves before (left panels) addition of Lat-A and the inhibition of waves after addition of 250 nM Lat-A (images shown are 80 s after LatA addition). (**E**) Comparison of actin wave speeds at a low dose (100 nM) of Lat-A with wave speeds in the absence of Lat-A. (**F**) TIRF images of an EGFP-actin cell showing actin waves as the cell spreads out before the addition of Jasplakinolide (− Jasp, left panel) and the loss of actin waves after addition of Jasplakinolide (+ Jasp, right panel, 6 min after drug addition). Scale bar is 10 μm. (**G**) Kymograph along a radial line across the periphery of a spreading EGFP-actin cell shows the effect of Jasplakinolide (Jasp). Addition of Jasp, shown by the yellow arrow, ∼2 min after the initiation of spreading stabilized the cell edge against retractions, and slowed down the cell edge. White arrow indicates the direction of time. Horizontal scale bar: 5 μm. Vertical scale bar: 2 min. (**H**) Time-lapse TIRF images of cells labeled with EGFP-actin with expression of myosin IIA heavy chain (Myh9) suppressed using siRNA. Actin waves are seen to emerge and propagate from multiple regions in the cell, similar to wild type cells. Scale bar is 5 μm. [Color figure can be viewed in the online issue, which is available at wileyonlinelibrary.com.]

the actin intensity and the edge velocity was similar to the control case (Fig. 6G, blue curve), suggesting that the mechanisms linking polymerization and membrane movement were similar both in the presence and absence of VCAM. We next characterized how VCAM affected the organization of actin regulators at the cell substrate interface. We found that the bursts and waves of Abi1 intensity in the interior of the cell were abolished in the presence of VCAM in contrast to control cells. Instead, YFP-Abi1 accumulated only in a narrow rim at the leading edge of the cell (Fig. 6H, Supporting Information, Movie S9).

As cells spread on the surface and establish actin rich lamellipodia, actin polymerization serves to push the membrane outwards while the actin at the periphery undergoes

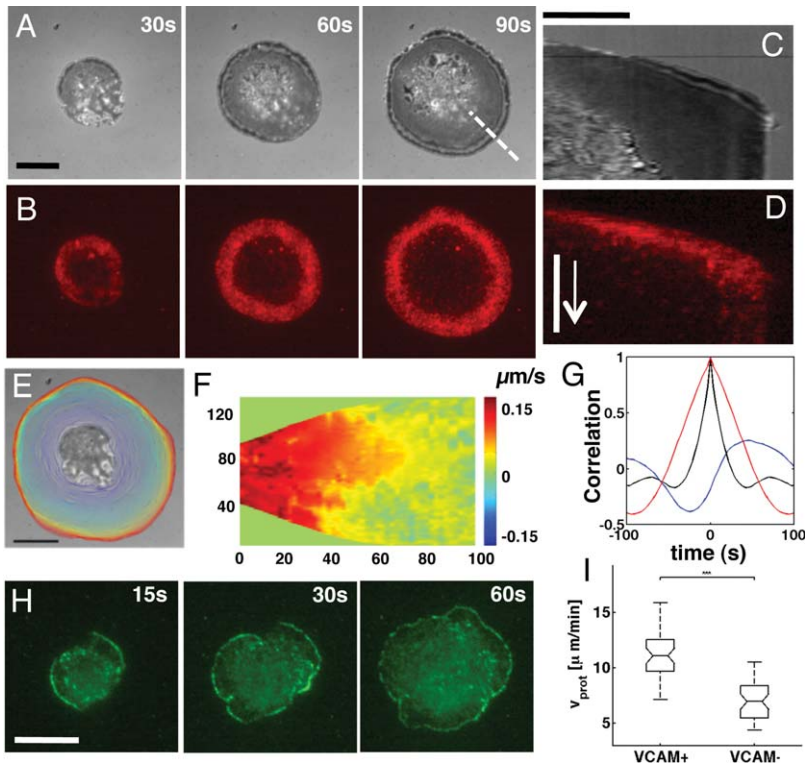

Fig. 6. VCAM modifies leading edge and actin dynamics: (**A**) Time-lapse IRM images of a cell spreading on a substrate coated with anti-CD3 antibody as well as VCAM. The IRM images show symmetric advance of the cell periphery and a uniform intensity level depicting a flat interface. Scale bar: 10 μm. (**B**) TIRF images of the same EGFP-actin cell shows that cells spreading on VCAM-coated substrates do not display actin waves. (**C**, **D**) Kymograph along a radial line [dashed line in (A)] of the IRM (A) and TIRF (D) time-lapse movie shows a smooth progression of the leading edge with no protrusion/retraction cycles. Horizontal scale bar: 5 μm. Vertical scale bar: 2 min. Direction of arrow indicates time. (**E**) Successive cell contours of a spreading cell reconstructed using active contours. 50 frames sampled every 2 s are shown. Cold colors indicate earlier times while warm colors indicate later times. Scale bar is 10 μm. (**F**) Space-time heat map of edge velocities in a direction normal to the cell edge computed using a level set algorithm from the reconstructed contours in (E). The peak protrusion velocities are ∼150 nm/s (red regions). (**G**) Temporal autocorrelation of the edge velocity (red), actin intensity (black), and the cross-correlation of the two (blue). (**H**) Time-lapse images of EYFP-Abi1-labeled cells spreading on a substrate coated with anti-CD3 and VCAM. Scale bar is 10 μm. (**I**) Cells spreading on anti-CD3+VCAM show significantly enhanced protrusion velocities as measured by kymography ($n = 26$ kymographs from 10 cells) compared to cells spreading on anti-CD3 alone ($n = 42$ kymographs from 11 cells) ($P < 0.001$, Wilcoxon's rank sum test).

retrograde flow toward the cell center. The protrusion speeds are determined by both the polymerization velocity and retrograde flow (protrusion = polymerization – retrograde flow). While we observed robust actin retrograde flow in control cells as quantified by kymography (8.0 ± 2.1 μm/min, $N = 18$), the retrograde flow of actin was inhibited (or very slow) on anti-CD3 and VCAM-coated substrates (Supporting Information, Fig. S2). Furthermore, the average protrusion velocity in the absence of VCAM was found to be 7.1 ± 1.8 μm/min ($N = 42$) which was significantly smaller than the average protrusion velocity for cells spreading on VCAM-coated substrates (11.1 ± 2.4 μm/min, $N = 26$, $P < 0.001$, Wilcoxon rank-sum test, Fig. 6I).

Previous studies have noted that the interaction between actin and TCR is dynamic, indicative of coordination between the two [Smoligovets et al., 2012]. To examine whether TCR/actin interactions at microclusters depended on VCAM-mediated adhesion, we next examined the temporal dynamics of actin intensities in the vicinity of identified microclusters. Figure 7A shows a representative cell spreading on anti-CD3 substrates. Kymographs along a radial line (Fig. 7B) show the appearance of ZAP70 clusters (green streaks) seconds after the appearance of actin (red). We show the normalized fluorescence intensity for both actin and ZAP70 (Fig. 7C) for the boxed region indicated in Fig. 7A. The EYFP-ZAP70 intensity rapidly increased with the formation of a microcluster, accompanied by an increase in Tag-RFP-T-actin fluorescence. While the rise in EYFP-ZAP70 fluorescence was over the same time scale as the actin fluorescence, the decline in EYFP fluorescence is likely due to a combination of steady-state exchange of ZAP70 between the cluster and the cytosol as well as photobleaching. The increase in ZAP70 intensity was transient, returning to background levels of fluorescence (Fig. 7C). Strikingly, we found that the actin fluorescence intensity oscillated irregularly and their intensity was significantly larger than fluctuations in the background intensity. To better characterize the spatio-temporal dynamics of actin, we quantified the temporal

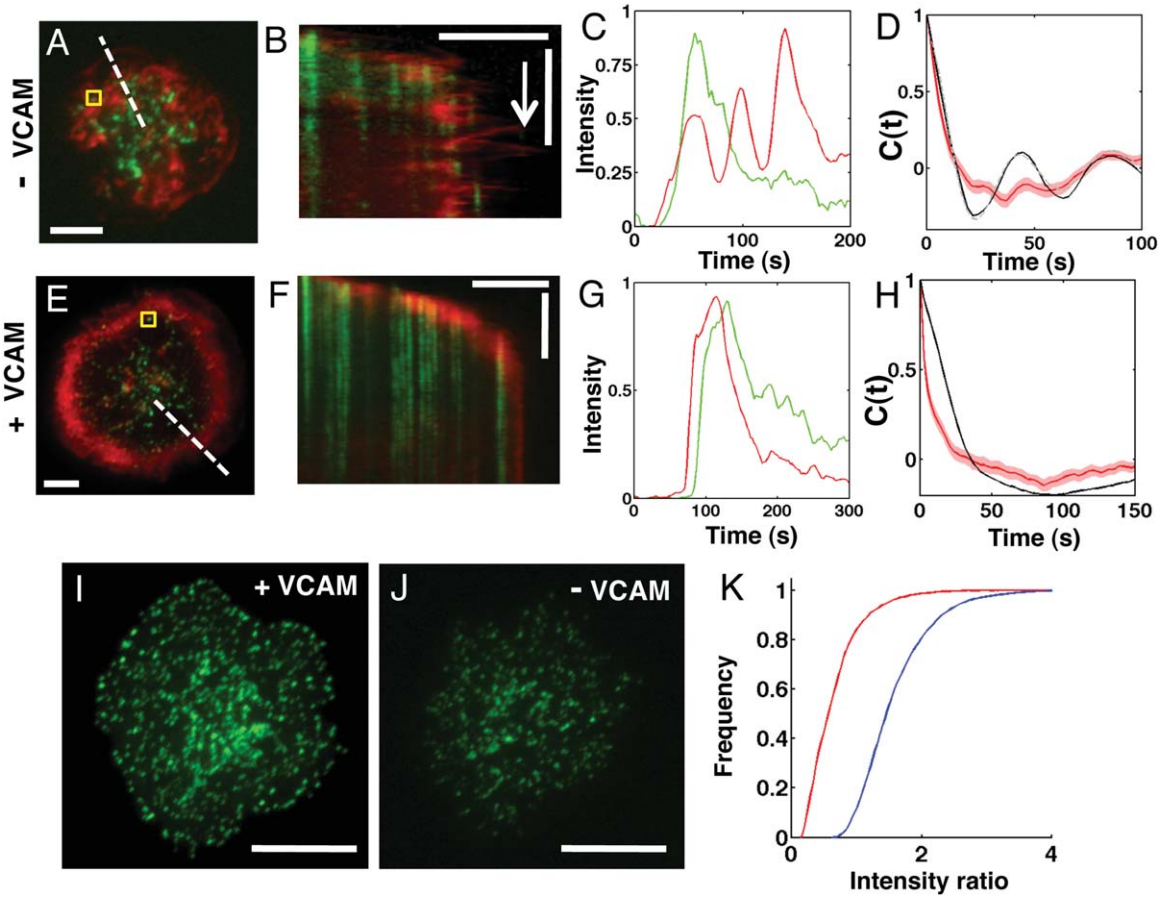

Fig. 7. Actin dynamics near signaling microclusters in the absence and presence of VCAM. (**A**) Representative image of a cell expressing EYFP-ZAP70 (green) and TagRFP-T-actin (red) 3 min after plating on anti-CD3 coated substrate. Boxed region shows a microcluster of ZAP70. (**B**) Representative kymograph along the radial dashed line in (A) indicating successive actin waves (red streaks), and clusters being formed at wave edges. Scale bars are: horizontal 5 μm; vertical 2 min. (**C**) Normalized integrated fluorescence intensity of ZAP70 (green) and actin (red) for the boxed region in (A) as a function of time. ZAP70 shows a rapid onset coincident with the formation of the microcluster. Actin intensity peaks at the same time but shows pronounced oscillations while ZAP70 fluorescence decays over 1 min. (**D**) Black curve shows the temporal autocorrelation of the actin intensity profile in (C). Red curve shows the autocorrelation of a region adjacent to the boxed region devoid of ZAP 70 clusters and the shaded regions show the 95% confidence interval for the correlation of the background intensity. The dashed line is a best fit to a damped cosine function $e^{-t}/_{\tau}\cos\omega t$ with $\tau = 30$ s and $\omega = 72$ s. The secondary peaks and dips are above the 95% confidence region of the background, indicating significant oscillatory correlations. (**E**) Representative image of a cell expressing EYFP-ZAP70 and TagRFP-T-actin spreading on VCAM and anti-CD3 coated substrate 3 min after plating. (**F**) A representative kymograph along the radial dashed line shows a smoothly advancing actin-rich lamellipodia (red), and clusters (green) forming at the cell periphery. Scale bars are: horizontal 5 μm; vertical 2 min. (**G**) Normalized integrated fluorescence intensity for ZAP70 (green) and actin (red) for the boxed region shown in (E). (**H**) Temporal autocorrelation of actin fluorescence region shown in (E): black curve; background region: red and 95% confidence interval: pink-shaded region. The fluorescence is best fit by an exponentially decaying function with a time constant of 30 s. (**I**) TIRF image of a dual-labeled cell spread on a substrate coated with VCAM and anti-CD3 showing EYFP-ZAP70 fluorescence. (**J**) TIRF image of a dual-labeled cell spread on a substrate coated with anti-CD3 showing EYFP-ZAP70 fluorescence. Scale bar is 5 μm for I, J. (**K**) Cumulative histogram of the ratio of cluster intensity to the mean ZAP70 fluorescence intensity in the cell contact zone for cells on substrates coated with anti-CD3 + VCAM (blue) and cells on substrates with anti-CD3 alone (red).

autocorrelation of TagRFP-T-actin intensity fluctuations in the vicinity of ZAP70 clusters. We found that the mean pixel-wise autocorrelation of the actin intensity fluctuations in a 1.5 × 1.5 micron region in the vicinity of the clusters. The computed autocorrelation clearly reflected the oscillatory nature of actin intensity fluctuations, as it was best fit by a damped cosine function (time constant ~30 s) and a period of ~72s, consistent with the observed edge oscillations (Fig. 7D, black curve). In contrast, the intensity fluctuations in regions with no discernable ZAP70 clusters and located away from clusters (Fig. 7D, red curve) showed no long-range temporal correlations. This pattern of correlation lends further support to our observations that actin oscillations emerge in the vicinity of signaling microclusters.

While VLA-4 ligation resulted in global alterations of actin dynamics (Fig. 6), it may also have an effect on actin dynamics near signaling clusters, by virtue of its effect on SLP-76 signaling [Nguyen et al., 2008]. We therefore

investigated the role of VCAM on the formation of signaling microclusters and the associated actin dynamics on substrates coated with both VCAM as well as anti-CD3. The fluorescence intensity of actin around the site of a cluster increased rapidly as the actin rich periphery advanced into the region (Figs. 7E and 7F). However, the actin fluorescence intensity rapidly decreased in time rather than display the oscillatory behavior observed in the absence of VCAM (Fig. 7G). Because TagRFP-T is considerably more photostable than EYFP [Shaner et al., 2008], this decline is unlikely to be due to photobleaching. A temporal autocorrelation plot of intensity fluctuations showed an exponential decay with a characteristic timescale of 30 s (Fig. 7H, black curve). Across the population ($n = 15$ cells for each substrate), we found that the actin intensity fluctuations in cells spreading on substrates coated with anti-CD3 alone were better fit by a damped cosine function, indicative of irregular oscillations in actin intensity, whereas a single exponential served as a better fit for cells spreading on anti-CD3+VCAM substrates, suggestive of transient accumulations of actin that rapidly dissipated. Note that in both cases, the actin fluorescence in regions devoid of clusters fluctuated on a much smaller scale around a background value. Finally, we examined whether the modulation of actin dynamics in the presence of VCAM results from integrin signaling or enhanced adhesion. We studied cells spreading on substrates coated with both anti-CD3 and anti-CD43 (a nonstimulatory adhesive ligand). TIRF imaging of TagRFP-T-actin and EYFP-ZAP70 showed waves of actin emerging from ZAP70 microclusters in spreading cells (Supporting Information, Fig. S3). This suggests that the modulation of actin dynamics, including inhibition of waves and oscillations, is specific to VCAM and likely at least in part mediated by signaling downstream of integrins.

Given our observations of differences in actin dynamics in the vicinity of microclusters on the two types of substrates (anti-CD3 +/− VCAM), and as actin dynamics is essential for proper microcluster assembly [Varma et al., 2006; Babich et al., 2012], we reasoned that the accumulation of signaling molecules in the microclusters would also be distinct. To quantify this, we computed the ratio of integrated fluorescence intensities of ZAP70 clusters (Fig. 7I, J) to the mean fluorescence intensity of the cell-substrate contact zone, an effective measure of the efficiency of cluster formation. On anti-CD3+ VCAM substrates, on which actin accumulation was transient, we found that ZAP70 clusters had a significantly higher intensity ratio, compared to those in cells spreading on substrates with anti-CD3 alone (Fig. 7K). Given the rough membrane topography of these cells on anti-CD3 alone, TIRF illumination would result in a higher intensity ratio, contrary to what we observe. Thus, it is likely that the differences are not due to imaging conditions. This suggests that the observed differences are due to distinct accumulation pattern of ZAP70 within the microclusters and correlated with the distinct pattern of actin dynamics.

Discussion

We have used live cell imaging and quantitative analysis to characterize actin dynamics during early stages of activation and microcluster formation. We found that actin and the regulatory protein Abi1 organize into rich spatiotemporal patterns such as traveling waves, moving spots, and spirals that originate at signaling microclusters. These structures require actin polymerization and depolymerization for their maintenance. Remarkably, these structures only occur when the membrane interface is rough, as adhesion to VCAM, which results in a smooth interface, abolished the waves, and actin intensity oscillations. We also found that integrin signaling resulted in distinct effects on actin dynamics in the vicinity of microclusters, suggesting the patterning of the actin network by TCR signaling may depend on the stimulatory environment. Without integrin engagement, repeated rounds of actin assembly accompanied the formation of microclusters, whereas in the presence of VCAM, actin enrichment was more transient. These differences were correlated with the accumulation of signaling proteins at microclusters, suggesting that actin dynamics may in turn serve to modulate signaling assemblies.

Actin waves have been observed in *Dictyostelium* [Vicker, 2002; Bretschneider et al., 2004; Gerisch et al., 2004] and in motile neutrophils during chemotaxis [Weiner et al., 2007]. However, the mobile actin structures we have characterized here in Jurkat cells appear to be distinct from those previously observed. First, TCR activation is obligatory for the formation of the propagating actin waves, unlike in *Dictyostelium* where waves are generated in the absence of G-protein signaling [Bretschneider et al., 2009]. Second, inhibition of actin polymerization arrests and disassembles the propagating waves of Abi1. In contrast, in neutrophils, the accumulation of Hem-1 (a component of the WAVE complex of proteins in hematopoetic cells) is enhanced on inhibition of actin polymerization, indicating that actin assembly leads to the detachment of the Hem-1 complex [Weiner et al., 2007], thus acting as a negative feedback for wave formation and propagation. Third, actin waves in Jurkat cells appear to be associated with membrane undulations and correlated with moving membrane folds suggesting that a coupling between chemical and mechanical factors is required to generate these waves. Finally, integrin signaling appears to abolish these waves. Previous studies on Jurkat, mouse, and human T cells have not reported such patterns, possibly because these studies either focused on well spread cells in the later stages of spreading or imaged the actin fluorescence using confocal microscopy which has lower axial resolution than TIRF microscopy [Bunnell et al., 2001; Gomez et al., 2006; Kaizuka et al., 2007; Babich et al., 2012]. Moreover, most studies of T cell spreading on lipid bilayers used ICAM-1 as an adhesive ligand, which may have suppressed such waves.

Modeling studies have suggested that actin-nucleating factors and filamentous actin can self-organize to form spatiotemporal structures such as waves, spots, and spirals [Gov and Gopinathan, 2006; Shlomovitz and Gov, 2008; Whitelam et al., 2009; Carlsson, 2010; Doubrovinski and Kruse, 2011; Ryan et al., 2012b]. Our results place specific constraints on models that can describe these phenomena. Specifically, given our observations that the membrane undulations at the cell substrate interface are severely reduced while waves are abolished on VCAM-coated substrates, we suggest that the regulation of membrane topography by adhesion may play a critical role in establishing these dynamic actin structures. The highly curved regions of the membrane may accumulate curvature-sensitive activators of Rho-GTPases [Aspenstrom, 2009; Suetsugu and Gautreau, 2012]. We hypothesize that the resulting actin polymerization may sustain or enhance membrane curvature, leading to a positive feedback between actin and its regulators [Rohatgi et al., 2001; Eden et al., 2002]. Membrane curvature may also lead to the accumulation of proteins that suppress actin regulators [Soderling et al., 2002] providing the negative feedback required for the formation of waves [Ryan et al., 2012b]. Another factor that might influence membrane curvature would be the membrane tension [Gov and Gopinathan, 2006; Shlomovitz and Gov, 2007]. Large values of tension would suppress membrane deformations, but intermediate values of tension may affect the wave velocity. Doubrovinski and Kruse [2011] have recently proposed a unified model that incorporates membrane elasticity, adhesion, and a dynamic actin cytoskeleton that exhibits traveling waves and moving spots of actin densities for certain choice of parameters as well as oscillations of the leading edge in spreading cells. Another model more directly linking membrane curvature to waves has been recently proposed for circular dorsal ruffles [Peleg et al., 2011]. Extending these models to include adhesion and signaling clusters as localized sources of activation may provide further insights into the actin dynamics in Jurkat T cells.

In addition to actin waves, we also observed dynamic protrusions and retractions of the cell edge, which were modulated by the presence of integrin mediated adhesion. Theoretical models of leading edge fluctuations [Ryan et al., 2012b] and propagating actin patterns have implicated actin polymerization as the main driver of the protrusions while the retractions are postulated to arise as a result of myosin contraction [Shlomovitz and Gov, 2007], global depolymerization, or the inhibition of actin nucleators by F-actin [Carlsson, 2012; Holmes et al., 2012]. However, the involvement of cell-substrate adhesion in the generation of the protrusion-retraction cycle is not very clear. Wolgemuth [2005] proposed a stick-slip model wherein contraction triggered by the buildup of osmotic stress resulting from actin depolymerization is opposed by cell-substrate adhesion. Weakly adhesive substrates offer minimal resistance resulting in the slippage of the cell edge, whereas stronger adhesion keeps the leading edge in place while the actin gel reassembles. Accordingly, we find that the $\alpha_4\beta_1$ integrin ligand, VCAM, leads to a persistent expansion of the cell edge, lending support to this model. Also consistent with the model, stabilization of the actin filaments against depolymerization by Jasplakinolide abolishes the edge retraction and leads to a stably moving lamellipodium at slightly reduced velocities. These differences may contribute to hematopoetic cell function. Thymocytes expressing VLA-4 exhibit less-centralized multifocal synapses [Balamuth et al., 2001; Leitenberg et al., 2001; Hailman et al., 2002], which may result from differences in actin dynamics. Similarly, VLA-4/VCAM ligation allows leukocytes to stabilize adhesion and resist detachment forces in an actin-dependent manner [Rullo et al., 2012]. Consistent with this, we found that the protrusion velocity was enhanced while actin retrograde flow was dramatically reduced on VLA-4/VCAM ligation. We suggest that similar to other adherent cells, integrins may provide a "clutch" like mechanism, which when engaged, can utilize all the force generated by actin polymerization to drive protrusion [Ponti et al., 2005; Hu et al., 2007].

The central role played by the actin cytoskeleton in T cell signaling has been demonstrated by pharmacological, physical, and genetic perturbations [Yu et al., 2013]. Collectively, these studies suggest that a dynamic actin network is required for effective TCR-ligand interaction as well as the formation and transport of kinases, scaffolds, and other proteins into micron-sized signaling assemblies around activated TCRs, but the coordinated behavior of the cytoskeletal network and signaling components is not well understood. Our quantitative analysis of actin dynamics during the very early stages of junction formation between a T lymphocyte and a stimulatory surface shows that the signaling microclusters intricately regulate actin dynamics both locally, in the vicinity of the cluster, and globally across the entire cell. A combination of TCR stimulation and VLA-4 mediated integrin signaling (costimulation) potentially creates an optimal balance of actin dynamics and signaling activation. Our results show that the actin cytoskeleton and regulatory proteins in Jurkat T cells couple with membrane undulations to lead to traveling waves, which are modulated by TCR and integrin signaling during activation. The dynamic edge oscillations under conditions of low adhesion and the actin coupled membrane waves may be helpful in the search for antigens on the relatively rough surface of an antigen presenting cell.

Materials and Methods

Cell Culture and Reagents

E6-1 Jurkat T cells (WT, stably transfected with EGFP-actin, Zap70-EYFP) were a gift from the lab of L. Samelson (NCI, NIH). TagRFP-T sequence was cloned from pcass

TagRFP-T (a gift from Dr. Morgan Huse, Rockefeller) into pEGFP-actin (Clontech, Mountain View, CA), using NheI and BspEI restrictions, to create pTagRFP-T-actin. The resultant construct was then digested by NotI and BamHI and cloned into Z4-MSCV-TagRFP-T (a gift from Dr. Morgan Huse, Rockefeller) to create Z4-MSCV-TagRFP-T-actin, allowing retroviral bicistronic expression of TagRFP-T-actin and a zeocin resistant gene. Retroviruses were generated according to standard protocol with Phoenix Amphotropic cells and were transduced into Jurkat cells by spin infection. The cells were then selected in 200 μg/mL zeocin for 2 weeks, and sorted with FACS to obtain high expression clones. Monoclonal cell lines were finally generated by limiting dilution of the sorted polyclonal population. TagRFP-T was introduced into WT E6-1 cells to generate TagRFP-T-actin cell line, and into Zap70-EYFP E6-1 cells to generate stable dual-color cell lines. pEYFP-Abi1 was a kind gift of Dr. Orion Weiner (UCSF). The plasmid was electroporated into E6-1 cells according to manufacturer's instructions.

E6-1 Jurkat T cells were cultured using standard protocols [Bunnell et al., 2001; Barda-Saad et al., 2005; Nguyen et al., 2008]. Briefly, cells were grown in RPMI 1640 medium supplemented with 10% fetal bovine serum at 37°C in a CO_2 incubator. Before imaging, 1 mL of cells was centrifuged at 240 × *g* for 5 min. The supernatant was removed and the cells were resuspended in imaging buffer similar to published protocols (4, 11; L-15 CO_2-independent medium, Invitrogen, Carlsbad, CA supplemented with 10% FBS). For drug inhibitions and treatments, the appropriate amount of reagent: Latrunculin-A, Jasplakinolide, and Blebbistatin (all purchased from Sigma-Aldrich, St. Louis, MO) was added to the imaging buffer. Cells were incubated at 37°C for 10 min before imaging.

Substrate Preparation and Imaging

Chambered coverslips were cleaned with 1 M HCl and 70% Ethanol for 30 min and dried at 37°C for 1 h. Chambers were treated for 10 min with 0.01% (weight/volume) poly-L-lysine solution (Sigma-Aldrich, St. Louis, MO), drained and dried for 1 h at 37°C. Chambers were coated with 10 μg/mL anti-CD3 antibody (Hit-3a, eBiosciences, San Diego, CA) for 2 h at 37°C. Excess antibody was removed by extensive washing with PBS. For coating with integrin ligands, VCAM was added to the dish at the indicated concentrations after antibody coating was completed. Cells were seeded on to chambers in the appropriate imaging medium. Fluorescence and IRM images were collected using an inverted microscope (TE2000 PFS, Nikon, Melville, NY) with a cooled CCD camera (Coolsnap HQ2, Photometrics, Tucson, AZ). TIRF imaging was done with a 60 × 1.49 NA objective lens, a 491-nm laser (100 mW, Andor, South Windsor, CT) for EGFP/EYFP excitation and a 561-nm laser (75 mW, Andor) for Tag-RFP excitation. Typical exposure times used for TIRF imaging was 200 ms, and time intervals for movies ranged from 1 to 3 s between frames.

Image Analysis

Cell Boundary Extraction

Cell boundaries were extracted using techniques detailed earlier [Lam Hui et al., 2012]. An active contour (snake algorithm) was applied to perform curvature-driven smoothing of the perimeter of the binary image and any self-intersections were removed.

Calculation of Edge Velocities

The level-set method offers a powerful way to extract leading edge normal velocities from successively sampled cell contours, while ensuring that the computed contours and edge velocities are topologically accurate [Machacek and Danuser, 2006]. However, high spatial resolution of images requires the solution of hyperbolic partial differential equations on very fine spatial grids, which can be computationally prohibitive. We used a simplified version of the Machacek–Danuser algorithm while maintaining the basic level set framework. First, coarse distance maps, which assign the distance of every grid point from successively sampled cell contours at time t and $t + dt$ were computed using the MATLAB (Mathworks, Natick, MA) function *bwdist*. A signed distance map was computed from the difference of these two distance functions using the fast marching method [Sethian, 1999]. A reinitialization procedure was performed to ensure that the signed distance map remained a true distance function. The resulting distance map is the normal distance from the contour at time t to that at $t+dt$, that is, the amount that marker points on the contour at t need to be advected by in order to lie on the next contour. We ensured that the Frobenius norm r of the difference between the distance function computed from the advected marker points (the computed contour at $t+dt$) and the original contour at $t+dt$ lay below a fixed threshold. As a cross-check, we verified that the direct solution of the level set PDEs using a fourth-order total variation diminishing Runge–Kutta scheme [Osher and Fedkiw, 2003] using a speed function computed above yielded similar results to our simplified procedure.

Actin Intensity Correlations

For analysis of ZAP70 clusters, the image was denoised using Wiener filtering and clusters were isolated using the *atrous* wavelet algorithm [Jaqaman et al., 2008]. A five-point rolling average was used to detrend the data. The pixelwise autocorrelation of the temporal intensity fluctuations was computed for an 11 × 11 pixel (1.2 μm^2) region around cluster centroids and averaged. For each cell, 20–50 clusters were used for the computation. A similar window was placed over regions with no identified ZAP70 clusters

to calculate temporal autocorrelations in sites with no TCR signaling. Jacknife statistics (3× variance of leave-one-out ∼95% confidence interval) were used to generate confidence intervals for autocorrelation functions.

Acknowledgments

The authors thank L. Samelson for providing the cell lines used here and useful discussions, Lakshmi Balagopalan-Bhise for help with the cell culture protocols, and Payam Fathi for technical assistance. This work was supported by the NSF (Grant numbers 1121710 and 1206060 to AU).

References

Asano Y, Nagasaki A, Uyeda TQ. 2008. Correlated waves of actin filaments and PIP3 in Dictyostelium cells. Cell Motil Cytoskeleton 65(12):923–934.

Aspenstrom P. 2009. Roles of F-BAR/PCH proteins in the regulation of membrane dynamics and actin reorganization. Int Rev Cell Mol Biol 272:1–31.

Babich A, Li S, O'Connor RS, Milone MC, Freedman BD, Burkhardt JK. 2012. F-actin polymerization and retrograde flow drive sustained PLCgamma1 signaling during T cell activation. J Cell Biol 197(6):775–787.

Balamuth F, Leitenberg D, Unternaehrer J, Mellman I, Bottomly K. 2001. Distinct patterns of membrane microdomain partitioning in Th1 and th2 cells. Immunity 15(5):729–738.

Barda-Saad M, Braiman A, Titerence R, Bunnell SC, Barr VA, Samelson LE. 2005. Dynamic molecular interactions linking the T cell antigen receptor to the actin cytoskeleton. Nat Immunol 6(1): 80–89.

Beemiller P, Krummel MF. 2010. Mediation of T-cell activation by actin meshworks. Cold Spring Harb Perspect Biol 2(9):a002444.

Beemiller P, Jacobelli J, Krummel MF. 2012. Integration of the movement of signaling microclusters with cellular motility in immunological synapses. Nat Immunol 13(8):787–795.

Billadeau DD, Nolz JC, Gomez TS. 2007. Regulation of T-cell activation by the cytoskeleton. Nat Rev Immunol 7(2):131–143.

Bretschneider T, Diez S, Anderson K, Heuser J, Clarke M, Muller-Taubenberger A, Kohler J, Gerisch G. 2004. Dynamic actin patterns and Arp2/3 assembly at the substrate-attached surface of motile cells. Curr Biol 14(1):1–10.

Bretschneider T, Anderson K, Ecke M, Muller-Taubenberger A, Schroth-Diez B, Ishikawa-Ankerhold HC, Gerisch G. 2009. The three-dimensional dynamics of actin waves, a model of cytoskeletal self-organization. Biophys J 96(7):2888–2900.

Bubb MR, Senderowicz AM, Sausville EA, Duncan KL, Korn ED. 1994. Jasplakinolide, a cytotoxic natural product, induces actin polymerization and competitively inhibits the binding of phalloidin to F-actin. J Biol Chem 269(21):14869–14871.

Bunnell SC, Kapoor V, Trible RP, Zhang W, Samelson LE. 2001. Dynamic actin polymerization drives T cell receptor-induced spreading: a role for the signal transduction adaptor LAT. Immunity 14(3):315–329.

Bunnell SC, Hong DI, Kardon JR, Yamazaki T, McGlade CJ, Barr VA, Samelson LE. 2002. T cell receptor ligation induces the formation of dynamically regulated signaling assemblies. J Cell Biol 158(7):1263–1275.

Burkhardt JK, Carrizosa E, Shaffer MH. 2008. The actin cytoskeleton in T cell activation. Annu Rev Immunol 26:233–259.

Campi G, Varma R, Dustin ML. 2005. Actin and agonist MHC-peptide complex-dependent T cell receptor microclusters as scaffolds for signaling. J Exp Med 202(8):1031–1036.

Carlsson AE. 2010. Dendritic actin filament nucleation causes traveling waves and patches. Phys Rev Lett 104(22):228102.

Carlsson AE. 2012. Self-feedback in actin polymerization. Adv Exp Med Biol 736:397–406.

Case LB, Waterman CM. 2011. Adhesive F-actin waves: a novel integrin-mediated adhesion complex coupled to ventral actin polymerization. PLoS One 6(11):e26631.

Dobereiner HG, Dubin-Thaler BJ, Hofman JM, Xenias HS, Sims TN, Giannone G, Dustin ML, Wiggins CH, Sheetz MP. 2006. Lateral membrane waves constitute a universal dynamic pattern of motile cells. Phys Rev Lett 97(3):038102.

Doubrovinski K, Kruse K. 2011. Cell motility resulting from spontaneous polymerization waves. Phys Rev Lett 107(25):258103.

Doucey MA, Legler DF, Faroudi M, Boucheron N, Baumgaertner P, Naeher D, Cebecauer M, Hudrisier D, Ruegg C, Palmer E,et al. 2003. The beta1 and beta3 integrins promote T cell receptor-mediated cytotoxic T lymphocyte activation. J Biol Chem 278(29): 26983–26991.

Douglass AD, Vale RD. 2005. Single-molecule microscopy reveals plasma membrane microdomains created by protein-protein networks that exclude or trap signaling molecules in T cells. Cell 121(6):937–950.

Dustin ML, Groves JT. 2012. Receptor signaling clusters in the immune synapse. Annu Rev Biophys 41:543–556.

Eden S, Rohatgi R, Podtelejnikov AV, Mann M, Kirschner MW. 2002. Mechanism of regulation of WAVE1-induced actin nucleation by Rac1 and Nck. Nature 418(6899):790–793.

Gerisch G, Bretschneider T, Muller-Taubenberger A, Simmeth E, Ecke M, Diez S, Anderson K. 2004. Mobile actin clusters and traveling waves in cells recovering from actin depolymerization. Biophys J 87(5):3493–3503.

Gerisch G, Ecke M, Schroth-Diez B, Gerwig S, Engel U, Maddera L, Clarke M. 2009. Self-organizing actin waves as planar phagocytic cup structures. Cell Adh Migr 3(4):373–382.

Goley ED, Welch MD. 2006. The ARP2/3 complex: an actin nucleator comes of age. Nat Rev Mol Cell Biol 7(10):713–726.

Gomez TS, McCarney SD, Carrizosa E, Labno CM, Comiskey EO, Nolz JC, Zhu P, Freedman BD, Clark MR, Rawlings DJ, et al. 2006. HS1 functions as an essential actin-regulatory adaptor protein at the immune synapse. Immunity 24(6):741–752.

Gov NS, Gopinathan A. 2006. Dynamics of membranes driven by actin polymerization. Biophys J 90(2):454–469.

Grakoui A, Bromley SK, Sumen C, Davis MM, Shaw AS, Allen PM, Dustin ML. 1999. The immunological synapse: a molecular machine controlling T cell activation. Science 285(5425):221–227.

Hailman E, Burack WR, Shaw AS, Dustin ML, Allen PM. 2002. Immature CD4(+)CD8(+) thymocytes form a multifocal immunological synapse with sustained tyrosine phosphorylation. Immunity 16(6):839–848.

Holmes WR, Carlsson AE, Edelstein-Keshet L. 2012. Regimes of wave type patterning driven by refractory actin feedback: transition from static polarization to dynamic wave behaviour. Phys Biol 9(4):046005.

Houtman JC, Houghtling RA, Barda-Saad M, Toda Y, Samelson LE. 2005. Early phosphorylation kinetics of proteins involved in proximal TCR-mediated signaling pathways. J Immunol 175(4): 2449–2458.

Hu K, Ji L, Applegate KT, Danuser G, Waterman-Storer CM. 2007. Differential transmission of actin motion within focal adhesions. Science 315(5808):111–115.

Ilani T, Vasiliver-Shamis G, Vardhana S, Bretscher A, Dustin ML. 2009. T cell antigen receptor signaling and immunological synapse stability require myosin IIA. Nat Immunol 10(5):531–539.

Innocenti M, Gerboth S, Rottner K, Lai FP, Hertzog M, Stradal TE, Frittoli E, Didry D, Polo S, Disanza A, et al. 2005. Abi1 regulates the activity of N-WASP and WAVE in distinct actin-based processes. Nat Cell Biol 7(10):969–976.

Jacobelli J, Chmura SA, Buxton DB, Davis MM, Krummel MF. 2004. A single class II myosin modulates T cell motility and stopping, but not synapse formation. Nat Immunol 5(5):531–538.

Janmey PA, McCulloch CA. 2007. Cell mechanics: integrating cell responses to mechanical stimuli. Annu Rev Biomed Eng 9:1–34.

Jaqaman K, Loerke D, Mettlen M, Kuwata H, Grinstein S, Schmid SL, Danuser G. 2008. Robust single-particle tracking in live-cell time-lapse sequences. Nature methods 5(8):695–702.

Kaizuka Y, Douglass AD, Varma R, Dustin ML, Vale RD. 2007. Mechanisms for segregating T cell receptor and adhesion molecules during immunological synapse formation in Jurkat T cells. Proc Natl Acad Sci USA 104(51):20296–20301.

Kasza KE, Zallen JA. 2011. Dynamics and regulation of contractile actin-myosin networks in morphogenesis. Curr Opin Cell Biol 23(1):30–38.

Kasza KE, Rowat AC, Liu J, Angelini TE, Brangwynne CP, Koenderink GH, Weitz DA. 2007. The cell as a material. Curr Opin Cell Biol 19(1):101–107.

Lam Hui K, Wang C, Grooman B, Wayt J, Upadhyaya A. 2012. Membrane dynamics correlate with formation of signaling clusters during cell spreading. Biophys J 102(7):1524–1533.

Leitenberg D, Balamuth F, Bottomly K. 2001. Changes in the T cell receptor macromolecular signaling complex and membrane microdomains during T cell development and activation. Semin Immunol 13(2):129–138.

Machacek M, Danuser G. 2006. Morphodynamic profiling of protrusion phenotypes. Biophys J 90(4):1439–1452.

Monks CR, Freiberg BA, Kupfer H, Sciaky N, Kupfer A. 1998. Three-dimensional segregation of supramolecular activation clusters in T cells. Nature 395(6697):82–86.

Nguyen K, Sylvain NR, Bunnell SC. 2008. T cell costimulation via the integrin VLA-4 inhibits the actin-dependent centralization of signaling microclusters containing the adaptor SLP-76. Immunity 28(6):810–821.

Nolz JC, Gomez TS, Zhu P, Li S, Medeiros RB, Shimizu Y, Burkhardt JK, Freedman BD, Billadeau DD. 2006. The WAVE2 complex regulates actin cytoskeletal reorganization and CRAC-mediated calcium entry during T cell activation. Curr Biol 16(1): 24–34.

Osher S, Fedkiw RP. 2003. Level Set Methods and Dynamic Implicit Surfaces. New York: Springer. xiii, 273 p., 16 p. of plates p.

Peleg B, Disanza A, Scita G, Gov N. 2011. Propagating cell-membrane waves driven by curved activators of actin polymerization. PLoS One 6(4):e18635.

Ponti A, Matov A, Adams M, Gupton S, Waterman-Storer CM, Danuser G. 2005. Periodic patterns of actin turnover in lamellipodia and lamellae of migrating epithelial cells analyzed by quantitative Fluorescent Speckle Microscopy. Biophys J 89(5):3456–3469.

Rohatgi R, Nollau P, Ho HY, Kirschner MW, Mayer BJ. 2001. Nck and phosphatidylinositol 4,5-bisphosphate synergistically activate actin polymerization through the N-WASP-Arp2/3 pathway. J Biol Chem 276(28):26448–26452.

Rullo J, Becker H, Hyduk SJ, Wong JC, Digby G, Arora PD, Cano AP, Hartwig J, McCulloch CA, Cybulsky MI. 2012. Actin polymerization stabilizes alpha4beta1 integrin anchors that mediate monocyte adhesion. J Cell Biol 197(1):115–129.

Ryan GL, Petroccia HM, Watanabe N, Vavylonis D. 2012a. Excitable actin dynamics in lamellipodial protrusion and retraction. Biophys J 102(7):1493–1502.

Ryan GL, Watanabe N, Vavylonis D. 2012b. A review of models of fluctuating protrusion and retraction patterns at the leading edge of motile cells. Cytoskeleton (Hoboken) 69(4):195–206.

Schroth-Diez B, Gerwig S, Ecke M, Hegerl R, Diez S, Gerisch G. 2009. Propagating waves separate two states of actin organization in living cells. HFSP J 3(6):412–427.

Sethian JA. 1999. Level set methods and fast marching methods : evolving interfaces in computational geometry, fluid mechanics, computer vision, and materials science. Cambridge, New York: Cambridge University Press. xx, 378 p.

Shaner NC, Lin MZ, McKeown MR, Steinbach PA, Hazelwood KL, Davidson MW, Tsien RY. 2008. Improving the photostability of bright monomeric orange and red fluorescent proteins. Nat Methods 5(6):545–551.

Shlomovitz R, Gov NS. 2007. Membrane waves driven by actin and Myosin. Phys Rev Lett 98(16):168103.

Shlomovitz R, Gov NS. 2008. Exciting cytoskeleton-membrane waves. Phys Rev E Stat Nonlin Soft Matter Phys 78(4 Pt 1): 041911.

Smoligovets AA, Smith AW, Wu HJ, Petit RS, Groves JT. 2012. Characterization of dynamic actin associations with T-cell receptor microclusters in primary T cells. J Cell Sci 125(Pt 3):735–742.

Soderling SH. 2009. Grab your partner with both hands: cytoskeletal remodeling by Arp2/3 signaling. Sci Signal 2(55):pe5.

Soderling SH, Binns KL, Wayman GA, Davee SM, Ong SH, Pawson T, Scott JD. 2002. The WRP component of the WAVE-1 complex attenuates Rac-mediated signalling. Nat Cell Biol 4(12): 970–975.

Suetsugu S, Gautreau A. 2012. Synergistic BAR-NPF interactions in actin-driven membrane remodeling. Trends Cell Biol 22(3):141–150.

Udagawa T, Woodside DG, McIntyre BW. 1996. Alpha 4 beta 1 (CD49d/CD29) integrin costimulation of human T cells enhances transcription factor and cytokine induction in the absence of altered sensitivity to anti-CD3 stimulation. J Immunol 157(5): 1965–1972.

Varma R, Campi G, Yokosuka T, Saito T, Dustin ML. 2006. T cell receptor-proximal signals are sustained in peripheral microclusters and terminated in the central supramolecular activation cluster. Immunity 25(1):117–127.

Vicker MG. 2002. Eukaryotic cell locomotion depends on the propagation of self-organized reaction-diffusion waves and oscillations of actin filament assembly. Exp Cell Res 275(1):54–66.

Weiner OD, Marganski WA, Wu LF, Altschuler SJ, Kirschner MW. 2007. An actin-based wave generator organizes cell motility. PLoS Biol 5(9):e221.

Welch MD, Mullins RD. 2002. Cellular control of actin nucleation. Annu Rev Cell Dev Biol 18:247–288.

Whitelam S, Bretschneider T, Burroughs NJ. 2009. Transformation from spots to waves in a model of actin pattern formation. Phys Rev Lett 102(19):198103.

Wolgemuth CW. 2005. Lamellipodial contractions during crawling and spreading. Biophys J 89(3):1643–1649.

Wu J, Motto DG, Koretzky GA, Weiss A. 1996. Vav and SLP-76 interact and functionally cooperate in IL-2 gene activation. Immunity 4(6):593–602.

Wulfing C, Davis MM. 1998. A receptor/cytoskeletal movement triggered by costimulation during T cell activation. Science 282(5397):2266–2269.

Yi J, Wu XS, Crites T, Hammer JA 3rd. 2012. Actin retrograde flow and actomyosin II arc contraction drive receptor cluster dynamics at the immunological synapse in Jurkat T cells. Mol Biol Cell 23(5):834–852.

Yokosuka T, Sakata-Sogawa K, Kobayashi W, Hiroshima M, Hashimoto-Tane A, Tokunaga M, Dustin ML, Saito T. 2005. Newly generated T cell receptor microclusters initiate and sustain T cell activation by recruitment of Zap70 and SLP-76. Nat Immunol 6(12):1253–1262.

Yu CH, Wu HJ, Kaizuka Y, Vale RD, Groves JT. 2010. Altered actin centripetal retrograde flow in physically restricted immunological synapses. PLoS One 5(7):e11878.

Yu Y, Smoligovets AA, Groves JT. 2013. Modulation of T cell signaling by the actin cytoskeleton. J Cell Sci 126(Pt 5):1049–1058.

Zipfel PA, Bunnell SC, Witherow DS, Gu JJ, Chislock EM, Ring C, Pendergast AM. 2006. Role for the Abi/wave protein complex in T cell receptor-mediated proliferation and cytoskeletal remodeling. Curr Biol 16(1):35–46.